

## Heating by exciton and biexciton recombination in GaAs/AlGaAs quantum wells

V.V. Belykh\* and M.V. Kochiev

*P.N. Lebedev Physical Institute of the Russian Academy of Sciences, Moscow, 119991 Russia*

(Received 15 March 2015; Revised 21 May 2015; Published 27 July 2015)

A comprehensive experimental investigation of exciton and biexciton recombination in GaAs/AlGaAs quantum wells is presented. Exciton and biexciton recombination times are found to be 16 and 55 ps, respectively. A method of determining the dynamics of the exciton temperature is developed. It is shown that both exciton and biexciton recombination processes increase the exciton temperature by an amount as high as  $\sim 10$  K. These processes impose a new restriction on the possibility of exciton Bose-Einstein condensation and make impossible its achievement in a system of direct excitons in GaAs quantum wells even for resonantly excited exciton gas.

PACS numbers: 78.47.jd, 78.55.Cr, 78.67.De

doi:10.1103/PhysRevB.92.045307

## INTRODUCTION

Excitons in semiconductors are a simple and very convenient analog of an atomic system. Like atoms, excitons can form molecules (biexcitons [1]) and ions (trions [2]). The Rydberg energy and Bohr radius of excitons are  $\sim 10$  meV and  $\sim 10$  nm as compared to  $\sim 10$  eV and  $\sim 0.1$  nm for atoms. This makes excitons more susceptible to external fields and allows one to implement in the laboratory conditions that are achievable only at extreme places of the Universe for atoms. Examples include the stabilization of the electron-hole liquid by a magnetic field [3] and spatial separation of electrons and holes by an electric field in quantum wells (QWs), which makes excitons indirect, suppressing the formation of exciton complexes and enhancing exciton radiative lifetime [4–6].

The achievement of Bose-Einstein condensation (BEC) in a system of ultracold atoms two decades ago [7, 8] together with rapid progress in nanotechnology inspired the work which has led to the attainment of BEC in a system of spatially indirect excitons in QWs [9–11] and exciton polaritons in microcavities [12, 13]. Atomic BEC was achieved at temperatures of  $\sim 10^{-7}$  K, which comprises the main difficulty in the experiment. On the other hand, the BEC of excitons can be reached at temperatures of  $\sim 1$  K due to their much smaller effective mass compared to the atomic mass. Excitons inevitably interact with thermal reservoir, the lattice, through the emission and absorption of phonons, and exciton system cooling is accomplished via the lattice cooling. On the other hand, an atomic system can be left on its own in a magneto-optical trap without interaction with any thermal reservoir, and the temperature of such a system is decreased by laser and evaporative cooling techniques [14]. Similarly to atomic BEC, the achievement of exciton BEC suffers from inelastic exciton-exciton collisions leading to biexciton formation [1, 15–19] and even to collapse into electron-hole liquid [20–22]. The exciton system in direct gap semiconductors suffers also from radiative recombination. This is why exciton BEC was searched

for indirect excitons with suppressed recombination and Coulomb attraction.

So far, it was believed that the main effect of exciton radiative recombination and biexciton formation on BEC is the decrease of exciton population which can be faster than thermalization of the system with the lattice [10]. In this case, it would be possible to attain BEC for resonant excitation of cold gas of direct excitons within an exciton population lifetime which is  $\sim 0.5$  ns in GaAs QWs. This lifetime and even exciton recombination time [23] are longer than exciton thermalization time [24, 25]. However, so far, only coherence mediated by the exciting laser was observed for exciton gas at low densities [26–32], and no signatures of spontaneous coherence were reported for direct excitons, to the best of our knowledge. In this paper, we show that exciton and biexciton recombination leads to significant heating of the exciton system. This imposes a new restriction on the possibility of exciton BEC. In particular, recombination heating makes it impossible to achieve BEC in a system of direct excitons in GaAs QWs even for resonantly excited cold exciton gas.

First, we determine the exciton and biexciton recombination times in QWs. In previous studies, the exciton recombination time (radiative decay time of low-momenta radiative excitons) was extracted from the photoluminescence (PL) kinetics of resonantly created excitons using sophisticated models taking into account different scattering mechanisms [23, 33]. The exciton recombination time was also determined in four-wave mixing experiments [34] and calculated theoretically [35]. Here, by using exciton-resonant excitation with different polarizations and powers and also different temperatures, we clearly show contributions of different dephasing processes to the decay rate of the fast component in the PL kinetics and determine the exciton recombination time. The biexciton recombination time so far was determined only in four-wave mixing experiments [34] and calculated theoretically [36, 37]. In this study, we determine biexciton recombination time directly by observing the decay of biexciton PL and rise of exciton PL upon the resonant

excitation of biexcitons.

Heating by exciton recombination (evaporative optical heating) was considered previously theoretically for free carriers [38] and indirect excitons [39] in QWs. However, to study this effect experimentally, one has to measure fairly small temperature changes. Here, we develop and ground a sensitive method to determine the exciton temperature dynamics based on the temperature dependence of the exciton population decay rate. We show both theoretically and experimentally that, for the considered system of direct excitons, the exciton temperature is higher than the lattice temperature by  $\gtrsim 4$  K due to exciton recombination heating. Furthermore, we demonstrate that the formation of biexcitons followed by their recombination also contributes significantly to the heating of the system. With increasing excitation power, the temperature increases by an amount proportional to the ratio of the biexciton and exciton concentrations, and this amount becomes as high as  $\sim 10$  K.

## EXPERIMENTAL DETAILS

The sample under study is a GaAs/Al<sub>0.05</sub>Ga<sub>0.95</sub>As heterostructure with two shallow tunneling-isolated QWs of widths  $d = 3$  and 4 nm. The thickness of the Al<sub>0.05</sub>Ga<sub>0.95</sub>As barrier layer separating the QWs is 60 nm. Only states of the wider QW were excited and studied. The same sample was used in Ref. [40], where the formation of trions as a result of the preferential capture of one species of carriers into the QWs under above-barrier excitation was studied.

The sample is mounted in a He-vapor optical cryostat and excited by the radiation of a mode-locked Ti-sapphire laser generating a periodic train of 2.5-ps-long pulses at a repetition rate of 76 MHz. The excitation laser beam is focused into a 10- to 20- $\mu$ m spot on the sample surface using a 6-mm-focus micro-objective located in front of the sample surface so that the surface is near its focal plane. The PL is collected by the same micro-objective. The excitation beam was slightly misaligned with respect to the optical axis, which allows to block the direct reflection. The micro-objective is mounted on the sample holder inside the cryostat, which provides the good stability of the system against vibrations. The PL coming out from the cryostat is focused with a  $\sim 100$ -mm-focus lens to form a magnified image of the PL spot on the slit of a spectrometer coupled to a Hamamatsu streak camera. The slits of the spectrometer and streak camera selected the central region of the PL spot with homogeneous intensity distribution. In all experiments except those described in Section (Fig. 2), the excitation beam was linearly polarized and PL was registered in a perpendicular linear polarization. The spectral resolution is 0.2 – 0.5 meV. The temporal resolution is 5 – 20 ps, depending on the spectral resolution and the used time

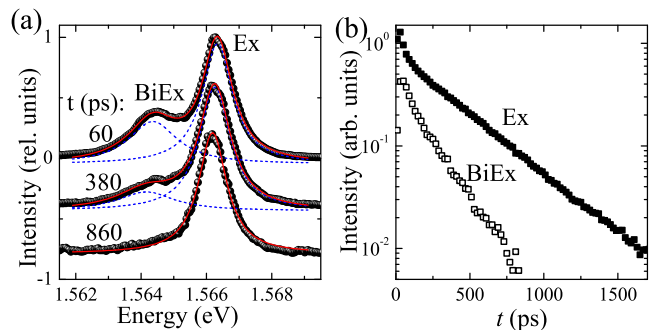


FIG. 1. (a) PL spectra, corresponding to the different times after the excitation pulse (symbols) fitted with Lorentzian peaks (lines). The spectra are normalized to the maximum value and vertically shifted. (b) Dynamics of the exciton (full symbols) and biexciton (open symbols) PL intensities. (a),(b) Exciton-resonant excitation ( $\Delta = 0$  meV) with  $P = 0.25$  mW,  $T_{\text{latt}} = 10$  K.

range.

## RESULTS AND DISCUSSION

The QW emission spectra for different times  $t$  after a resonant excitation pulse are presented in Fig. 1(a). The spectra feature two lines separated by about 2 meV. The higher-energy line (Ex) is attributed to exciton emission. It persists in the spectra even for sufficiently high temperatures and low e-h densities. The lower-energy line (BiEx) is significantly reduced with respect to the exciton line as the e-h density decays with time (Fig. 1(a)). We attribute this low-energy line to biexciton emission. Indeed, generation of biexcitons is the most efficient for the resonant excitation [15, 16]. The spectrum is fitted with two Lorentzian peaks (lines in Fig. 1(a)) to determine the intensities, widths, and spectral positions of the exciton and biexciton lines. The intensity of the BiEx line decays about two times faster than the intensity of the Ex line (Fig. 1(b)) as expected for biexcitons [17, 18], and the biexciton nature of the BiEx line will be further confirmed throughout the paper.

### Exciton recombination time

Here we determine the exciton recombination time (radiative decay time of low-momenta radiative excitons) by investigating the exciton dynamics with temporal resolution of about 5 ps for exciton-resonant linearly polarized excitation. Figure 2(a) shows exciton intensity dynamics registered in polarization parallel ( $\parallel$ , solid curves) and perpendicular ( $\perp$ , dashed curves) to the excitation polarization. Two decay components are clearly seen in the  $\parallel$  polarization kinetics, while the  $\perp$  polarization kinetics

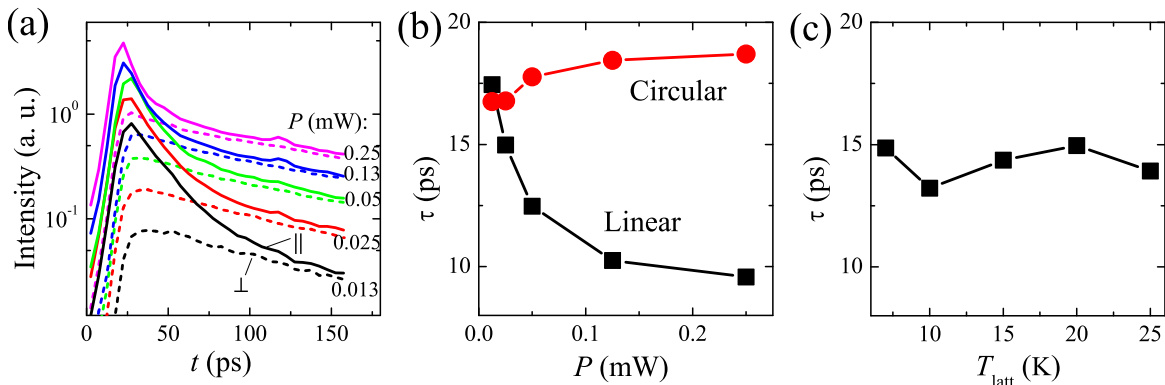


FIG. 2. Exciton-resonant excitation ( $\Delta = 0$  meV). (a) Exciton intensity dynamics in linear polarizations parallel (solid lines) and perpendicular (dashed lines) to the excitation polarization for different excitation powers.  $T_{\text{latt}} = 10$  K. (b) Power dependences of the fast component decay time for the linearly (squares) and circularly (circles) polarized excitations.  $T_{\text{latt}} = 10$  K. (c) Temperature dependence of the fast component decay time for linearly polarized excitation with  $P = 0.013$  mW (different excitation spot position on the sample).

shows the slow component only. We interpret these observations as follows. A resonant excitation pulse creates a large population of low- $k$  radiative excitons with wave vectors within the light-cone. Accordingly, the fast component is induced by the initial low- $k$  exciton recombination and scattering towards the nonradiative reservoir, while the slow component corresponds to the decay of the reservoir exciton population. The contribution of a spin relaxation to the decay of the fast component is small [34]. Otherwise, the PL decay in  $\parallel$  polarization would be accompanied by the comparable PL rise in the  $\perp$  polarization, which is not seen in the experiment (Fig. 2(a)). The initial scattering of the low- $k$  excitons to the nonradiative states corresponds to the increase of the mean exciton energy (temperature) either due to the absorption of phonons (the corresponding scattering rate is  $1/\tau_{\text{phon}}$ ) or to the formation of biexcitons (the corresponding rate is  $1/\tau_{\text{f}}$ ). Indeed, each biexciton formation event releases energy for the exciton system approximately equal to the biexciton binding energy. For the decay rate of the fast component neglecting the scattering back from the reservoir we can write  $1/\tau = 1/\tau_0 + 1/\tau_{\text{phon}} + 1/\tau_{\text{f}}$ . As the excitation density  $P$  is increased, the rate of biexciton formation increases and  $\tau$  should decrease, which we do observe in the experiment (black squares in Fig. 2(b)). In the limit of  $P \rightarrow 0$  we have  $1/\tau = 1/\tau_0 + 1/\tau_{\text{phon}}$ . Interestingly, for circularly polarized excitation, the fast component decay time for the co-polarized intensity is almost independent of  $P$ . This can be explained by the fact that biexciton formation is suppressed for circularly polarized exciton population since total biexciton spin equals zero [1, 41].

An increase in the lattice temperature  $T_{\text{latt}}$  should favor phonon absorption and lead to an increase in  $1/\tau_{\text{phon}}$ , causing a decrease in  $\tau$ . However, Fig. 2(c) shows that  $\tau$

is almost independent of  $T_{\text{latt}}$ , indicating that  $\tau_{\text{phon}} \gg \tau$ . As we show in the following, interaction with phonons is characterized by times of  $\sim 100$  ps. Note also that at low  $P$  secondary emission can preserve laser-mediated coherence for a time comparable to  $\tau_0$  [26–32], which, of course, does not prevent exciton radiative decay at the rate  $1/\tau_0$ . Finally, at small  $P$ ,  $\tau \approx \tau_0$  and we get the exciton recombination time  $\tau_0 \approx 16 \pm 2$  ps. This result is consistent with the results of kinetic measurements of Ref. [23] (10 ps for a 4.5-nm QW) and Ref. [33] (20 ps for an 8-nm QW), with four-wave mixing studies of Ref. [34] (13 ps for a 25-nm QW) and theoretical calculations Ref. [35] (25 ps for a 10-nm QW).

### Biexciton recombination time

Now we determine the biexciton recombination time (radiative lifetime) by investigating the exciton-biexciton dynamics with a temporal resolution of about 5 ps for biexciton-resonant linearly polarized excitation (Fig. 3). Biexciton-resonant excitation implies the absorption of two photons leading to the creation of a biexciton having an energy of  $2E_{\text{x}} - E_{\text{b}}$ . Thus, we used the excitation photon energy  $\hbar\omega = E_{\text{x}} - E_{\text{b}}/2$  detuned by  $\Delta = E_{\text{laser}} - E_{\text{x}} = -1$  meV from the exciton resonance. Figure 3 shows, that for this excitation energy, the biexciton intensity greatly exceeds the exciton intensity at short times. Then, the biexciton intensity rapidly decays with a characteristic time  $\tau_1 \approx 35$  ps. The decay of the biexciton intensity is accompanied by an increase in the exciton intensity, which starts to decrease at later times.

The simplest scenario explaining the experimental observations is the following. An excitation pulse creates biexciton population. In a process of biexciton radiative

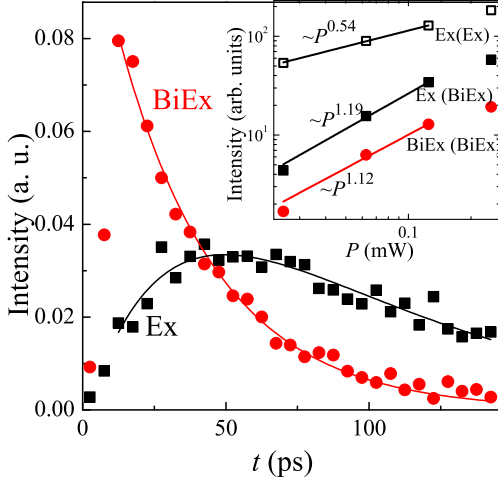


FIG. 3. Dynamics of exciton (squares) and biexciton (circles) PL intensities for biexciton-resonant excitation ( $\Delta = -1$  meV) with  $P = 0.13$  mW. The inset shows power dependences of the exciton (squares) and biexciton (circles) time-integrated intensities for biexciton-resonant (full symbols) and exciton-resonant (open symbols) excitations.  $T_{\text{latt}} = 10$  K.

decay, one of the e-h pairs constituting a biexciton recombines to give a photon with energy  $E_x - E_b$  and leaves an exciton. Thus, the radiative decay of biexciton population is accompanied by the creation of the same amount of excitons. Subsequently excitons either decay radiatively or form secondary biexcitons giving much weaker emission at longer times, so the latter process can be neglected. According to this scenario the time-integrated biexciton intensity should be equal to the time-integrated exciton intensity. In the experiment, however, the total exciton intensity exceeds the total biexciton intensity by a about factor of  $r \approx 3$  for all considered excitation powers (see the inset in Fig. 3, solid squares and circles, respectively). This fact indicates that excitons can be formed not only as a result of biexciton radiative decay, but also as a result of biexciton dissociation. Furthermore, the excitation pulse can create some initial exciton population which can be seen in Fig. 3 as a nonzero value of the exciton intensity corresponding to the maximal biexciton intensity. The inset in Fig. 3 demonstrates that both exciton and biexciton time-integrated intensities show almost identical power dependences, which at low  $P$  can be approximated by  $\propto P^{1.19}$  and  $\propto P^{1.12}$ , respectively, with the exponent about twice as large as that for the excitons upon exciton-resonant excitation ( $\propto P^{0.54}$ , open squares in the inset, the sublinear dependence might be related to the fact that we do not register the emission in the direction of the direct reflection of the resonant beam which shows a large secondary emission intensity within a few picoseconds [26]). These

$P$ -dependences confirm the fact that biexcitons are created by two-photon absorption process. Furthermore, the possible initial exciton population is also created by two-photon rather than by the standard one-photon absorption process. However, more likely all the excitons are created from decay or dissociation of biexcitons only, and the initial exciton population reflects the number of excitons created from biexcitons within our time resolution.

The dynamics of the exciton-biexciton system can be described by the following rate equations [17]:

$$\frac{dN_x}{dt} = -\frac{N_x}{\tau_x} + \frac{N_b}{\tau_b} + 2\frac{N_b}{\tau_d} - 2F(N_x), \quad (1)$$

$$\frac{dN_b}{dt} = -\frac{N_b}{\tau_b} - \frac{N_b}{\tau_d} + F(N_x), \quad (2)$$

where  $N_x$  and  $N_b$  are the exciton and biexciton concentrations, respectively;  $\tau_x$ ,  $\tau_b$ , and  $\tau_d$  are the times of the whole exciton population radiative decay, biexciton recombination, and biexciton dissociation, respectively; the term  $F(N_x)$  describes biexciton formation from two excitons. In the description of the fast stage we disregard the formation of secondary biexcitons described by the last term in both equations. This process determines the biexciton intensity when quasiequilibrium between exciton and biexciton populations is established. This intensity is much smaller than the biexciton intensity at the considered fast stage for the same level of the exciton intensity (compare Figs. 1(b) and 3). Equations (1) and (2) without the last term have the following solution:

$$N_x = N_b^0 \frac{2/\tau_1 - 1/\tau_b}{1/\tau_1 - 1/\tau_x} [(1 + \alpha)e^{-t/\tau_x} - e^{-t/\tau_1}], \quad (3)$$

$$N_b = N_b^0 e^{-t/\tau_1}, \quad (4)$$

where  $1/\tau_1 = 1/\tau_b + 1/\tau_d$  is the biexciton intensity decay time,  $N_b^0$  is the initial biexciton concentration, parameter  $\alpha \geq 0$  determines the initial exciton concentration:  $N_x^0 = \alpha N_b^0 (2/\tau_1 - 1/\tau_b) / (1/\tau_1 - 1/\tau_x)$ . It is easy to show that the ratio of the total time-integrated exciton intensity to the total biexciton intensity is

$$r = (2\frac{\tau_b}{\tau_1} - 1)(\alpha\frac{\tau_x}{\tau_x - \tau_1} + 1), \quad (5)$$

and, correspondingly, the expression for biexciton recombination time is

$$\tau_b = \frac{\tau_1}{2} [1 + r(\alpha\frac{\tau_x}{\tau_x - \tau_1} + 1)^{-1}]. \quad (6)$$

Thus,  $\tau_b \leq \tau_1(1+r)/2$ , and since  $1/\tau_1 = 1/\tau_b + 1/\tau_d$ ,  $\tau_b \geq \tau_1$ . For experimental values  $\tau_1 = 35$  ps and  $r = 2.9$  we have  $35 \leq \tau_b \leq 68$  ps. To get the more precise value of  $\tau_b$ , we extract  $\alpha = 0.17$  and  $\tau_x = 69$  ps (such a short  $\tau_x$  is related to the low exciton temperature in the first 100 ps) from the fit of the exciton intensity kinetics with Eq. (3). Finally we obtain the biexciton recombination time  $\tau_b = 55$  ps and dissociation time  $\tau_d = 94$  ps.

Interestingly, the biexciton recombination time  $\tau_b = 55$  ps is larger than the exciton recombination time  $\tau_0 = 16$  ps. However,  $\tau_0$  and  $\tau_b$  have different physical meanings. The exciton recombination time determines the rate of radiative decay of only low- $k$  radiative excitons, while the total exciton population, mainly consisting of nonradiative reservoir, decays at longer times  $\tau_x \sim 400$  ps, as it follows from the experiment (Fig. 1(b)) at  $t \gtrsim 200$  ps. On the other hand, biexciton radiative decay is allowed for any biexciton wave vector since it can be transmitted to the residual exciton. Thus,  $\tau_b$  determines the radiative decay of the whole biexciton population. The value  $\tau_b = 55$  ps  $>$   $\tau_0$  is compatible with theoretical results of Ref. [36], where  $\tau_b$  was calculated for all biexciton momenta. On the other hand, calculations performed for biexcitons with almost zero momentum within the giant oscillator strength model [37] as well as four-wave mixing experiments, which also probe almost zero-momentum biexcitons, [34] give somewhat smaller biexciton recombination times: 20 and 11 ps, respectively. The obtained value of  $\tau_b = 55$  ps is much smaller than the biexciton recombination time evaluated in Ref. [18] (330 ps) as the time of the biexciton intensity decay under intense nonresonant excitation in the assumption that the biexciton is the dominant species. As we will show later this assumption is not valid.

### Exciton-biexciton thermodynamics

Now, let us consider the behavior on the time scale  $t > \tau_0, \tau_b$ . One can easily estimate that, contrary to the common belief [18], the biexciton population is much smaller than the exciton one even for comparable exciton and biexciton intensities  $I_x \sim I_b$ :  $N_b/N_x \approx I_b\tau_b/I_x\tau_x \sim \tau_b/\tau_x \sim 55/400 \sim 0.1$ . Furthermore, taking into account the relatively slow change of the biexciton concentration  $dN_b/dt \approx 2N_b/t_x$  at the considered time scale (Fig. 1), it follows from Eqs. (1) and (2) that  $N_b \approx N_b^{\text{eq}}/(1 + \tau_d/\tau_b) \approx 0.4N_b^{\text{eq}}$ , where  $N_b^{\text{eq}} = \tau_d F(N_x)$  is the equilibrium biexciton concentration. Thus, the biexciton concentration is far from the equilibrium one due to the short radiative decay time of biexcitons compared to the biexciton formation/dissociation time. The biexciton population is driven by the excitons just like the nonequilibrium polariton population in a microcavity is driven by the exciton reservoir [42].

It is instructive to estimate the absolute value of the exciton density  $N_x$ . Poor knowledge of the QW absorption coefficient makes it difficult to determine  $N_x$  directly from the excitation density. For our estimates, we used the exciton line blue-shift which is, according to Ref. [43],  $\delta E \approx 3E_{\text{xb}}\lambda_{2\text{D}}^2 N_x$  (the detailed calculations of exciton-exciton interaction are given in Refs. [44, 45]), where  $E_{\text{xb}}$  is the exciton binding energy and  $\lambda_{2\text{D}}$  is the two-dimensional exciton Bohr radius defined as in Ref. [44].

For excitation power  $P = 0.25$  mW (Fig. 1) at the beginning of the kinetics  $\delta E \approx 0.2$  meV; taking  $E_{\text{xb}} = 7$  meV,  $\lambda_{2\text{D}} = 10$  nm, we obtain  $N_x \approx 10^{10}$  cm $^{-2}$ . The biexciton density can be determined from the exciton density in two ways: (i) From the ratio of the biexciton and exciton intensities as it was described above:  $N_b \approx N_x I_b \tau_b / I_x \tau_x$ . For  $N_x = 10^{10}$  cm $^{-2}$  and  $I_b/I_x = 0.4$  at the beginning of the kinetics for  $P = 0.25$  mW (Fig. 1) we obtain  $N_b \approx 0.6 \times 10^9$  cm $^{-2}$ . (ii) By calculating the equilibrium biexciton density  $N_b^{\text{eq}}$  corresponding to a given exciton density from the law of mass action [18]:

$$\frac{N_x^2}{N_b^{\text{eq}}} = \frac{g_x^2 m_x T}{4\pi\hbar^2} \exp(-E_b/T), \quad (7)$$

where  $m_x \approx 0.3 \times 10^{-27}$  g is the two dimensional exciton effective mass [46],  $g_x = 4$  is the exciton spin degeneracy, and we put  $k_B = 1$ . For  $N_x = 10^{10}$  cm $^{-2}$ ,  $T = 10$  K we obtain  $N_b^{\text{eq}} \approx 1.3 \times 10^9$  cm $^{-2}$ . As mentioned above, due to the short biexciton lifetime, actual biexciton density  $N_b \approx 0.4N_b^{\text{eq}} \approx 0.5 \times 10^9$  cm $^{-2}$ . Good agreement between biexciton densities calculated in two different ways justifies our estimate for the exciton density.

Although the ratio of the total biexciton and exciton concentrations is far from equilibrium, both exciton and biexciton momentum distributions should be close to the thermal distribution characterized by the internal temperature  $T$  in general not equal to the lattice temperature  $T_{\text{latt}}$ . This is true since the thermalization time determined by interparticle scattering at considered excitation densities is shorter than  $\tau_0$  and  $\tau_b$  [24, 25] (interparticle scattering time can be estimated from the homogeneous density-dependent broadening which is up to 1 meV in our experiments). Short thermalization time also excludes the effects related to the laser-mediated coherence which may be important only at low densities [26–32]. Furthermore, the estimated exciton density indicates that the exciton ensemble is nondegenerate at the considered temperatures and can be described by the classical Boltzmann distribution.

### Internal temperature dynamics

Now, we will describe how the internal temperature  $T$  of the exciton-biexciton system can be determined from the decay time of the exciton population  $\tau_x$ , and discuss the dynamics of  $T$ .

The radiative decay rate of the whole exciton population is given by the following relation:  $N_x/\tau_x = N_{\text{rad}}/\tau_0$ , where  $N_{\text{rad}}$  is the concentration of excitons in the radiative zone with wave vectors within the light cone  $k < \omega n/c$  and spins  $\pm 1$ . This concentration can be evaluated as  $N_{\text{rad}} \approx \delta E_r (1/2) f(0) D = \delta E_r N_x / 2T$ , where we put the energy of the bottom of the exciton dispersion curve to zero,  $\delta E_r = (\hbar\omega n/c)^2 / 2m_x \approx$

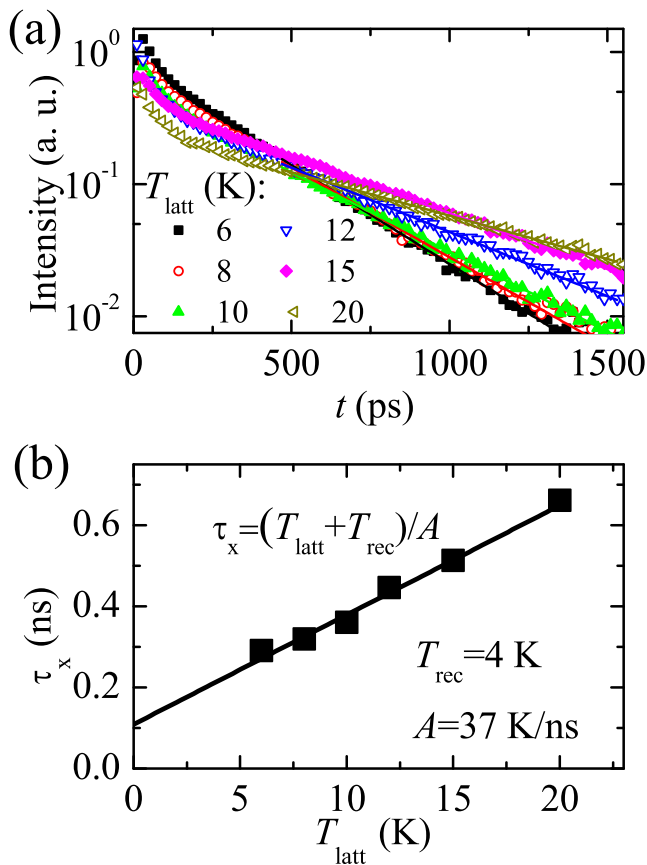


FIG. 4. (a) Dynamics of the exciton PL intensities (symbols) at different lattice temperatures for exciton-resonant excitation with  $P = 0.13$  mW. The lines show the exponential fits. (b) Lattice temperature dependence of the exciton PL decay time (symbols). The line shows the linear fit.

$80 \mu\text{eV}$  is the maximal energy of the radiative excitons,  $f(E) = (\pi\hbar^2 N_x / 2m_x T) \exp(-E/T)$  is the occupancy of exciton states given by the Boltzmann distribution,  $D = 2m_x / \pi\hbar^2$  is the exciton density of states per unit area,  $n \approx 3.3$  is the refractive index of the GaAs, and we used  $T \gg \delta E_r$ . Finally, for the radiative decay time of the whole exciton population we have

$$\tau_x = 2\tau_0 T / \delta E_r = \frac{T}{A}, \quad (8)$$

and we introduced phenomenological constant  $A = \delta E_r / 2\tau_0$  which will be determined in the experiment and related to the measured  $\tau_0$ .

Figure 4(a) shows the exciton PL kinetics at different lattice temperatures. At long times, the PL decay can be described by a monoexponential function and the decay time is equal  $\tau_x$  if we neglect biexciton formation. The dependence of  $\tau_x$  on  $T_{\text{latt}}$  is shown in Fig. 4(b). As expected, this dependence is linear  $\tau_x = (T_{\text{latt}} + T_{\text{rec}})/A$ , however, there is nonzero offset suggesting that the internal exciton temperature is higher than lattice temper-

ature by a constant value  $T_{\text{rec}} \approx 4$  K. The origin of  $T_{\text{rec}}$  will be discussed in the following. The experimental value  $A = 37$  K/ns corresponds to the exciton recombination time  $\tau_0 \approx 13$  ps in good agreement with measured value of 16 ps. The linear dependence of the exciton population decay time on temperature was also observed in previous experiments [Ref. [47] ( $A \approx 20$  K/ns for a 4-nm QW) and Ref. [48] ( $A \approx 45$  K/ns for a 4-nm QW)] and calculated theoretically [Ref. [35] ( $A \approx 29$  K/ns for a 10-nm QW)].

We have shown that the exciton internal temperature is proportional to the decay time of the exciton intensity (Eq. (8)). However, in the experiment the decay time can be defined unambiguously only at large times, when the intensity decay is exponential and the internal temperature almost reached its steady-state value. Now, we extract the internal temperature at any time  $T(t)$  from the dynamics of the exciton and biexciton intensities. The exciton intensity (defined as the number of particles emitted in the unit time)  $I_x(t) = N_x(t)/\tau_x(t) = AN_x(t)/T(t)$ . On the other hand,  $N_x(t) = \int_t^\infty (I_x(t') + I_b(t')) dt'$ , where we use  $N_b \ll N_x$ . Thus,

$$T(t) = A \frac{\int_t^\infty (I_x(t') + I_b(t')) dt'}{I_x(t)}. \quad (9)$$

This expression offers a method to determine the exciton temperature from the PL dynamics. In the case of monoexponential decay and when  $I_b(t) \ll I_x(t)$ , Eq. (9) is reduced to Eq. (8).

To test the validity of this method, we perform experiments using excitations with different excess energies  $\Delta = E_{\text{laser}} - E_x$  with respect to the exciton resonance, which defines the initial exciton temperature. The excitation density is relatively low, so the biexciton recombination heating (see following) is small (for  $\Delta < 0$  it is small at  $t \gtrsim \tau_b$ ). The exciton PL dynamics under excitation with different excess energies is shown in Fig. 5(a). Figure 5(b) shows the exciton temperature dynamics determined according to Eq. (9) from the measured exciton and biexciton intensity dynamics. As expected, the temperature relaxes from the value determined by the excess energy and reaches the steady-state value  $T_{\text{st}} = T_{\text{latt}} + T_{\text{rec}}$  at long times. The following qualitative criterion applies: the faster the intensity decrease, the lower the temperature and vice versa [compare curves in Figs. 5(a) and 5(b)]. Our method can be applied even for low exciton temperatures and concentrations, where the temperature can not be determined from the Boltzmann tail in the PL spectra, which originates either from the e-h plasma recombination [49] or from the longitudinal optical (LO) phonon replica of exciton recombination [50].

Now, we show that increase of the internal exciton temperature  $T$  by  $T_{\text{rec}}$  [offset of the dependence in Fig. 4(b)] is related to recombination heating [38] (evaporative optical heating [39]), a process similar to evaporative cooling in atomic systems [8, 14]. The average exciton energy is

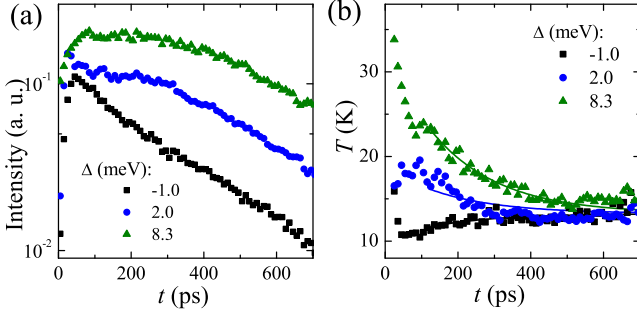


FIG. 5. Dynamics of the exciton intensity (a) and internal temperature (b) for excitations with different excess energies  $\Delta$  with respect to the exciton resonance and  $P = 0.13$  mW. Lines in Fig. 5(b) show exponential fits.  $T_{\text{latt}} = 10$  K.

$T$ , but only excitons with low energies  $< \delta E_r \ll T$  recombine; as a result, the average exciton energy is increased. Here, we disregard biexciton formation, which is insignificant at long times. To describe exciton recombination heating quantitatively, let us consider the evolution of the exciton system total energy per unit area  $N_x T$ :

$$\frac{d}{dt}(N_x T) = -\frac{N_x \delta E_r}{\tau_x} - \kappa(T - T_{\text{latt}})N_x. \quad (10)$$

The total energy changes due to the radiative decay (first term, where  $E_r/2$  is the average energy of recombining excitons) and due to the emission/absorption of phonons (second term). The latter process tends to equalize the temperatures of the exciton system and the lattice, so in the first-order approximation, its rate is proportional to  $T - T_{\text{latt}}$ . The proportionality coefficient  $\kappa$  characterizes the strength of the exciton-phonon interaction. Taking into account that  $dN_x/dt = -N_x/\tau_x = -AN_x/T$  and  $\delta E_r \ll T$ , we obtain the solution of Eq. (10):

$$T = T_0 e^{-\kappa t} + (T_{\text{latt}} + \frac{A}{\kappa})(1 - e^{-\kappa t}), \quad (11)$$

where  $T_0$  is the initial temperature. Thus, the steady-state value of the exciton temperature achieved at  $t \gg 1/\kappa$

$$T_{\text{st}} = T_{\text{latt}} + \frac{A}{\kappa} \quad (12)$$

is higher than  $T_{\text{latt}}$  by a constant  $T_{\text{rec}} = A/\kappa$ , in agreement with the results in Figs. 4(b) and 5(b). The recombination heating temperature

$$T_{\text{rec}} = \frac{A}{\kappa} = \frac{\delta E_r}{2\tau_0 \kappa} \quad (13)$$

is determined by the exciton recombination rate and exciton-phonon interaction constant. Interestingly, only interaction with the lattice prevents the temperature

from rising infinitely. By fitting the temperature dynamics in Fig. 5(b) with Eq. (11), we determine  $\kappa \approx 5.4 \text{ ns}^{-1}$  (exciton-phonon scattering time  $1/\kappa \approx 180$  ps), and we can calculate the recombination heating temperature  $T_{\text{rec}} = A/\kappa \approx 37/5.4 \approx 6.9$  K which is in a reasonable agreement with the value  $T_{\text{rec}} = 4$  K determined from the data in Fig. 4(b).

Another process that, in addition to exciton recombination heating, contributes to the increase in the exciton temperature is the formation of biexcitons with their *subsequent recombination*. Indeed, each biexciton formation event with subsequent recombination releases energy  $E_b$  for the exciton system, while the emitted photon has energy  $-E_b$ . Thus, taking into account that  $N_b \ll N_x$ , while intensities  $I_b = N_b/\tau_b$  and  $I_x = N_x/\tau_x$  might be comparable, one has to add a term  $E_b N_b/\tau_b$  to the right-hand side of Eq. (10). This term describes the energy increase due to biexciton recombination. As a result, the temperature dynamics is described by the equation

$$\frac{dT}{dt} = A - \kappa(T - T_{\text{latt}}) + \frac{E_b}{\tau_b} \frac{N_b}{N_x}, \quad (14)$$

leading to

$$T = T_0 e^{-\kappa t} + (T_{\text{latt}} + \frac{A}{\kappa})(1 - e^{-\kappa t}) + \frac{E_b}{\tau_b} \int_0^t \frac{N_b(t')}{N_x(t')} e^{-\kappa(t-t')} dt' \quad (15)$$

The last term determines the temperature increase due to biexciton recombination. To calculate this term, one should obtain the time dependence of  $N_x$  and  $N_b$  from Eqs. (1) and (2). However, the constants  $\tau_x$ ,  $\tau_d$  and formation rate  $F(N_x)$  in these equations in turn depend on  $T$ . To get an approximate expression for the last term in Eq. (15), we put  $N_x \propto \exp(-t/\tau_x)$  and  $N_b \propto \exp(-2t/\tau_x)$  and disregard the dependence of  $\tau_x$  on  $T$ . Finally,

$$T = T_0 e^{-\kappa t} + (T_{\text{latt}} + \frac{A}{\kappa})(1 - e^{-\kappa t}) + \frac{E_b}{\tau_b \kappa - \tau_b/\tau_x} \frac{I_b(0)}{I_x(0)} (e^{-t/\tau_x} - e^{-\kappa t}). \quad (16)$$

Thus, biexciton recombination can increase the internal temperature by as much as  $\sim E_b$ .

Figure 6(b) shows the exciton temperature dynamics for different powers of exciton-resonant excitation. The corresponding exciton and biexciton intensities are shown in Fig. 6(a). For the lowest excitation power, the temperature monotonously increases to the steady-state value  $T_{\text{st}}$ . On the other hand, for higher powers, when the biexciton intensity becomes comparable to the exciton intensity (Fig. 6(a)), the temperature first increases above  $T_{\text{st}}$  and then decreases to  $T_{\text{st}}$ . This initial temperature rise results from biexciton recombination heating and is proportional to  $I_b/I_x$ . As the biexciton intensity

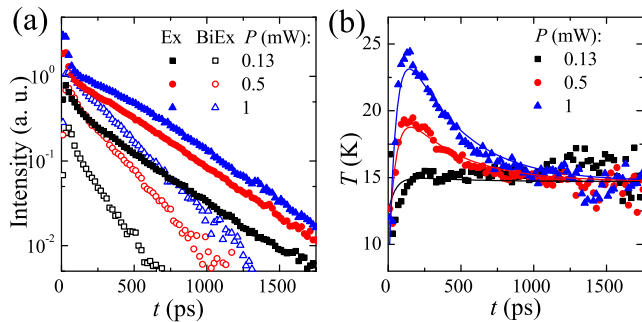


FIG. 6. Dynamics of the exciton (solid symbols) and biexciton (open symbols) intensities (a) and the internal temperature (b) for exciton-resonant excitation ( $\Delta = 0$ ) with different powers. Lines in Fig. 6(b) show biexponential fits.  $T_{\text{latt}} = 10$  K.

becomes much lower than the exciton intensity, the temperature relaxes to  $T_{\text{st}}$ . The dependences in Fig. 6(b) are fitted with double-exponential functions in accordance with Eq. (16) with the temperature decay time set to  $\tau_x = 0.38$  ns.

The described heating mechanisms cancel out the possibility of exciton BEC in the considered system even for resonant excitation. Indeed, the system temperature can not be lower than  $\sim 4$  K for a time longer than few tens of picoseconds even for  $T_{\text{latt}} = 0$ . This already gives a BEC threshold density of at least  $N_{\text{thr}} \sim 2m_x T_{\text{rec}}/\pi \approx 1.6 \times 10^{12} \text{ cm}^{-2}$  which is of the same level as the exciton saturation density  $N_{\text{sat}} \sim 1/a_B^2 \sim 10^{12} \text{ cm}^{-2}$ . Furthermore, an increase in the exciton density leads to a proportional increase in the temperature due to biexciton recombination heating  $T_b \propto N_b/N_x \propto N_x$ . Experiment shows that even a moderate increase in  $N_x$ , to the level when  $I_b$  becomes comparable to  $I_x$ , leads to an increase in  $T$  up to  $\sim 10$  K. This effect forbids exciton BEC even if one forgets about exciton saturation.

## CONCLUSION

A consistent picture of exciton and biexciton recombination in GaAs/AlGaAs quantum wells has been developed. The exciton recombination time has been determined to be  $\tau_0 = 16$  ps, while the radiative decay time of the whole exciton population including large-momentum nonradiative part is  $\tau_x = T/(37 \text{ K/ns}) \gg \tau_0$ . The biexciton recombination time, which also characterizes the radiative decay of the whole biexciton population, has been determined to be  $\tau_b = 55$  ps. As a result of  $\tau_b \ll \tau_x$ , the biexciton concentration is significantly lower than one would expect in thermal equilibrium. It is also much lower than the exciton concentration, while the exciton and biexciton emission intensities can be comparable. Thus, the main role of the biexciton states in

the thermodynamics of the whole system is that they provide an additional radiative channel for excitons.

A method of determining the temperature dynamics of the exciton system has been developed. It is based on the proportionality of the radiative decay time of the whole exciton population and temperature of the exciton system and also takes into account biexciton recombination channel. The method has been tested in experiments with different excess energies of the excitation photons which define the initial temperatures of the system.

The heating of the exciton system by exciton recombination has been analyzed theoretically and revealed in the experiment. This effect is analogous to evaporative cooling in atomic systems. An increase in the temperature due to recombination heating ( $\sim 4$  K in the QWs under study) is proportional to the exciton recombination rate and inversely proportional to the rate of cooling by acoustic phonons.

It has been shown that biexciton formation and subsequent recombination also lead to an increase in the exciton temperature by an amount proportional to the ratio of the biexciton and exciton emission intensities. For comparable biexciton and exciton intensities, this increase can be as large as tens of Kelvins.

The revealed recombination heating effects imply new restrictions on the Bose-Einstein condensation of excitons. These restrictions cancel out BEC in many exciton systems even where the thermalization rate exceeds the radiative decay rate (like direct excitons in GaAs/AlGaAs QWs) and even for resonantly created cold exciton gas.

The main quantitative conclusions of the paper are summarized in Table I.

We are grateful to M. L. Skorikov for careful reading of the manuscript, valuable remarks and advices, and to N. N. Sibeldin and V. A. Tsvetkov for useful discussions. The work is supported by the Russian Science Foundation (Project No. 14-12-01425).

Exciton recombination time	$\tau_0 = 16$ ps
Biexciton recombination time	$\tau_b = 55$ ps
Radiative decay time of the whole exciton population	$\tau_x = T/A$ , $A = 37$ K/ns
Exciton temperature dynamics	$T(t) = A[\int_t^\infty (I_x(t') + I_b(t'))dt']/I_x(t)$
Exciton recombination heating temperature	$T_{\text{rec}} = A/\kappa \approx 4$ K
Biexciton recombination heating temperature	$T_b = (E_b/\tau_b) \int_0^t [N_b(t')/N_x(t')] \exp[-\kappa(t-t')]dt'$

TABLE I. Summary of the main quantitative results.

- \* belykh@lebedev.ru; present address: Experimentelle Physik 2, Technische Universität Dortmund, 44227 Dortmund, Germany
- [1] R. C. Miller, D. A. Kleinman, A. C. Gossard, and O. Munteanu, *Phys. Rev. B* **25**, 6545 (1982).
- [2] K. Kheng, R. T. Cox, M. Y. d'Aubigné, F. Bassani, K. Saminadayar, and S. Tatarenko, *Phys. Rev. Lett.* **71**, 1752 (1993).
- [3] I. V. Kavetskaya, N. N. Sibeldin, and V. A. Tsvetkov, *Solid State Commun.* **97**, 157 (1996).
- [4] A. Alexandrou, J. A. Kash, E. E. Mendez, M. Zachau, J. M. Hong, T. Fukuzawa, and Y. Hase, *Phys. Rev. B* **42**, 9225 (1990).
- [5] K. Sivalertporn, L. Mouchliadis, A. L. Ivanov, R. Philp, and E. A. Mulyarov, *Phys. Rev. B* **85**, 045207 (2012).
- [6] G. J. Schinner, J. Repp, E. Schubert, A. K. Rai, D. Reuter, A. D. Wieck, A. O. Govorov, A. W. Holleitner, and J. P. Kotthaus, *Phys. Rev. Lett.* **110**, 127403 (2013).
- [7] M. H. Anderson, J. R. Ensher, M. R. Matthews, C. E. Wieman, and E. A. Cornell, *Science* **269**, 198 (1995).
- [8] K. B. Davis, M. O. Mewes, M. R. Andrews, N. J. Van Druten, D. S. Durfee, D. M. Kurn, and W. Ketterle, *Phys. Rev. Lett.* **75**, 3969 (1995).
- [9] L. V. Butov, A. C. Gossard, and D. S. Chemla, *Nature* **418**, 751 (2002).
- [10] A. A. High, J. R. Leonard, A. T. Hammack, M. M. Fogler, L. V. Butov, A. V. Kavokin, K. L. Campman, and A. C. Gossard, *Nature* **483**, 584 (2012).
- [11] A. V. Gorbunov and V. B. Timofeev, *JETP Lett.* **96**, 138 (2012).
- [12] J. Kasprzak, M. Richard, S. Kundermann, a. Baas, P. Jeambrun, J. M. J. Keeling, F. M. Marchetti, M. H. Szymaska, R. André, J. L. Staehli, V. Savona, P. B. Littlewood, B. Deveaud, and L. S. Dang, *Nature* **443**, 409 (2006).
- [13] R. Balili, V. Hartwell, D. Snoke, L. Pfeiffer, and K. West, *Science* **316**, 1007 (2007).
- [14] E. A. Cornell and C. E. Wieman, *Rev. Mod. Phys.* **74**, 875 (2002).
- [15] D. J. Lovering, R. T. Phillips, G. J. Denton, and G. W. Smith, *Phys. Rev. Lett.* **68**, 1880 (1992).
- [16] R. T. Phillips, D. J. Lovering, G. J. Denton, and G. W. Smith, *Phys. Rev. B* **45**, 4308 (1992).
- [17] J. C. Kim, D. R. Wake, and J. P. Wolfe, *Phys. Rev. B* **50**, 15099 (1994).
- [18] J. C. Kim and J. P. Wolfe, *Phys. Rev. B* **57**, 9861 (1998).
- [19] M. Mootz, M. Kira, S. W. Koch, A. E. Almand-Hunter, and S. T. Cundiff, *Phys. Rev. B* **89**, 155301 (2014).
- [20] C. D. Jeffries and L. V. Keldysh, *Electron-Hole Droplets Semicond.* (North Holland, Amsterdam, 1983).
- [21] T. M. Burbaev, E. A. Bobrik, V. A. Kurbatov, M. M. Rzaev, N. N. Sibeldin, V. A. Tsvetkov, and F. Schäffler, *JETP Lett.* **85**, 331 (2007).
- [22] V. S. Bagaev, V. S. Krivobok, S. N. Nikolaev, A. V. Novikov, E. E. Onishchenko, and M. L. Skorikov, *Phys. Rev. B* **82**, 115313 (2010).
- [23] B. Deveaud, F. Clérot, N. Roy, K. Satzke, B. Sermage, and D. S. Katzer, *Phys. Rev. Lett.* **67**, 2355 (1991).
- [24] W. H. Knox, C. Hirlimann, D. A. B. Miller, J. Shah, D. S. Chemla, and C. V. Shank, *Phys. Rev. Lett.* **56**, 1191 (1986).
- [25] W. H. Knox, D. S. Chemla, G. Livescu, J. E. Cunningham, and J. E. Henry, *Phys. Rev. Lett.* **61**, 1290 (1988).
- [26] S. Haacke, R. A. Taylor, R. Zimmermann, I. Bar-Joseph, and B. Deveaud, *Phys. Rev. Lett.* **78**, 2228 (1997).
- [27] N. Garro, M. J. Snelling, S. P. Kennedy, R. T. Phillips, and K. H. Ploog, *Phys. Rev. B* **60**, 4497 (1999).
- [28] W. Langbein, R. Zimmermann, E. Runge, and J. Hvam, *Physica Status Solidi B* **221**, 349 (2000).
- [29] G. R. Hayes, B. Deveaud, V. Savona, and S. Haacke, *Phys. Rev. B* **62**, 6952 (2000).
- [30] V. Savona, E. Runge, and R. Zimmermann, *Phys. Rev. B* **62**, R4805 (2000).
- [31] G. Kocherscheidt, W. Langbein, U. Woggon, V. Savona, R. Zimmermann, D. Reuter, and A. D. Wieck, *Phys. Rev. B* **68**, 085207 (2003).
- [32] V. Savona and E. Runge, *Physica Status Solidi B* **234**, 9 (2002).
- [33] A. Vinattieri, J. Shah, T. C. Damen, D. S. Kim, L. N. Pfeiffer, M. Z. Maialle, and L. J. Sham, *Phys. Rev. B* **50**, 10868 (1994).
- [34] W. Langbein and J. M. Hvam, *Phys. Rev. B* **61**, 1692 (2000).
- [35] L. C. Andreani, F. Tassone, and F. Bassani, *Solid State Commun.* **77**, 641 (1991).
- [36] D. S. Citrin, *Phys. Rev. B* **50**, 17655 (1994).
- [37] A. L. Ivanov, H. Wang, J. Shah, T. C. Damen, L. V. Keldysh, H. Haug, and L. N. Pfeiffer, *Phys. Rev. B* **56**, 3941 (1997).
- [38] D. Bimberg and J. Mycielski, *Phys. Rev. B* **31**, 5490 (1985).
- [39] A. L. Ivanov, *J. Phys. Condens. Matter* **16**, S3629 (2004).
- [40] M. V. Kochiev, V. A. Tsvetkov, and N. N. Sibeldin, *JETP Lett.* **95**, 481 (2012).
- [41] S. B.-T. De-Leon and B. Laikhtman, *Europhys. Lett.* **59**, 728 (2002).
- [42] V. V. Belykh and D. N. Sob'yanin, *Phys. Rev. B* **89**, 245312 (2014).

- [43] S. Schmitt-Rink, D. S. Chemla, and D. A. B. Miller, *Phys. Rev. B* **32**, 6601 (1985).
- [44] C. Ciuti, V. Savona, C. Piermarocchi, A. Quattropani, and P. Schwendimann, *Phys. Rev. B* **58**, 7926 (1998).
- [45] S. B.-T. De-Leon and B. Laikhtman, *Phys. Rev. B* **63**, 125306 (2001).
- [46] H. Hillmer, A. Forchel, S. Hansmann, M. Morohashi, E. Lopez, H. P. Meier, and K. Ploog, *Phys. Rev. B* **39**, 10901 (1989).
- [47] J. Feldmann, G. Peter, E. O. Göbel, P. Dawson, K. Moore, C. Foxon, and R. J. Elliott, *Phys. Rev. Lett.* **59**, 2337 (1987).
- [48] J. Martinez-Pastor, A. Vinattieri, L. Carraresi, M. Colocci, P. Roussignol, and G. Weimann, *Phys. Rev. B* **47**, 10456 (1993).
- [49] J. Szczytko, L. Kappei, J. Berney, F. Morier-Genoud, M. T. Portella-Oberli, and B. Deveaud, *Phys. Rev. Lett.* **93**, 137401 (2004).
- [50] S. Bieker, T. Henn, T. Kiessling, W. Ossau, and L. W. Molenkamp, *Phys. Rev. B* **90**, 201305(R) (2014).